Power-law correlations and finite-size effects in silica particle aggregates studied by small-angle neutron scattering

T. Freltoft and J. K. Kjems
Physics Department, Risø National Laboratory, DK-4000 Roskilde, Denmark

S. K. Sinha
Science Laboratories, Exxon Research and Engineering Corporation, Clinton Township, Route 22 East, Annandale, New Jersey 08801
(Received 11 July 1985)

Small-angle neutron scattering from normal, compressed, and water-suspended powders of aggregates of fine silica particles has been studied. The samples possessed average densities ranging from 0.008 to 0.45 g/cm^3. Assuming power-law correlations between particles and a finite correlation length ξ, we derive the scattering function $S(q)$ from specific models for particle-particle correlation in these systems. $S(q)$ was found to provide a satisfactory fit to the data for all samples studied. The fractal dimension d_f corresponding to the power-law correlation was 2.61 ± 0.1 for all dry samples, and 2.34 ± 0.1 for the water-suspended samples. The intensity of scattering was found to scale with the correlation length in the manner expected for a fractal system.

I. INTRODUCTION

The clustering of small particles into large ramified objects is a commonly occurring phenomena. In biological systems one finds protein aggregation, in colloid and polymer chemistry one finds coagulation, flocculation, and gel formation, and in metallurgy one finds a range of nucleation and growth processes, all of which can be treated theoretically in terms of kinetic models of the kind first discussed by Smoluchowski.[1]

The recent efforts in this field have been stimulated by the observation that the resulting clusters often show a considerable, and quite remarkable, degree of self-similarity or scale invariance. In particular, the work by Forest and Witten[2] on silica smoke particles and the subsequent computer simulations by Witten and Sander,[3,4] who devised the simple, elegant diffusion-limited–aggregation (DLA) model, have started an avalanche of both experimental the theoretical work which seeks a quantitative understanding of the aggregation processes.

An important and fundamental parameter in the description of the geometrical arrangement of the particles in a scale-invariant cluster is called the fractal dimension,[5] d_f, loosely identified as the Hausdorff-Besikowitch dimension, which describes how the mass of the cluster increases with its linear dimension r,

$$M(r)\propto r^{d_f},\quad d_f<d\ .$$

Contrary to what is found in normal condensed-matter systems, the exponent d_f can take on noninteger values between 1 and the embedding dimension d.

In this paper we will describe how scattering experiments can be used to determine d_f and we will present experimental results obtained by small-angle neutron scattering from low-density powders of silica smoke particles which are available commercially under the trade names Cab-O-Sil and Alfasil.[6] They are produced by the process of flame hydrolysis in which $SiCl_4$ is burned to give a snowlike product in which the basic small-particle units are amorphous SiO_2 spheres roughly 5 nm in diameter. A preliminary account of these experiments has been published previously.[7] Similar diffraction studies of colloidal silica aggregates formed in suspensions have been reported by Schaefer *et al.*,[8] who used x-ray and light scattering to obtain the diffraction profiles. They were able to determine the fractal dimension $d_f=2.1$ from their data. The process of colloidal aggregation has also been studied by Weitz *et al.*,[9,10] who used electron microscopy to characterize the geometry and have subsequently confirmed their values for d_f by diffraction experiments using light, x-ray, and neutron scattering.

Diffraction experiments probe the density correlations on length scales which correspond to the inverse momentum transfer q^{-1}, and since the intensity per particle scales with the correlated mass in the probing volume, it is to be expected that the intensity scales as q^{-d_f}. However, as will be discussed later, in real physical systems the scale invariance is limited to a finite range between upper and lower bounds. These limits will be treated explicitly in this paper and we will demonstrate how they can be incorporated in the theoretical expressions for the scattering law one expects from a sample consisting of finite-size aggregates.

The paper is organized in the following manner: First, we describe the small-angle neutron scattering experiments we have carried out on compressed powders and on suspended samples of Cab-O-Sil and Alfasil silica aggregates. We then develop the scattering theory for such systems and, finally, analyze our scattering data and extract the relevant structural parameters as the fractal dimension and the upper and lower cutoff lengths from fits to the data. Finally, we discuss to what extent the data are really consistent with a fractal model of the aggregates.

II. EXPERIMENTAL DETAILS

A. Samples

The commercial products Cab-O-Sil and Alfasil are produced by hydrolysis of silicon tetrachloride vapor in a flame of hydrogen and oxygen. The production process has been studied in detail by Ulrich and Riehl.[11] They measured the aggregate mass by a light scattering technique as a function of growth time in a number of cases, varying both the SiO_2 concentration in the flame and the burner type.

Three sets of samples were prepared for the present experiments based on commercially available material. Samples with densities ranging from 0.05 to 0.2 g/cm^3 were made by packing the materials in 1- and 2-mm-thick cuvettes. Samples with densities up to 0.5 g/cm^3 were made by pressing equal amounts of material into 20-mm disks using a hydraulic press. Note that the highest density studied was still much lower than that of bulk silica ($\approx$2.5 g/cm^3). Suspended samples were prepared by mixing 2 wt. % Cab-O-Sil with water of different $[H_2O]/[D_2O]$ ratios and decanting the liquid after centrifugation, yielding low concentrations of the aggregates ($\approx$0.006–0.008 g/cm^3). The samples with different contrasts $[H_2O]/[D_2O]$ ratio) were investigated to ensure that aggregates were entirely dispersed, i.e., that no enclosed air remained in closed pores giving rise to additional scattering.

B. Experiment

The experiments were carried out at the small-angle neutron scattering (SANS) facility[12] at the Risø DR-3 reactor. The SANS instrument is situated in the neutron house at the end of a cold-neutron guide tube outside the reactor. A mechanical velocity filter consisting of a rotating drum with tilted slits selects a wavelength band from the continuous cold-source spectrum. For the present experiment wavelengths of 0.6 and 2.2 nm were used with $\Delta\lambda/\lambda=0.18$ FWHM (full width at half maximum). The first collimating slit (16 mm) and the monitor for the incident-neutron dose are situated behind the velocity selector. The distance to the second slit (8 mm) in the sample chamber was 2.25 m. A sample changer with holders for 1- or 2-mm-thick quartz cuvettes was used, and a pumping system at the sample position kept the pressure in the entire instrument from monitor to detector at 10^{-5} mbar. The distance from the sample to the area-sensitive detector was 3 m. The detector was a multiwire proportional ^{3}He detector[13] with an active area of 40×40 cm^2, in which three planes of wires mounted on fiberglass frames were used for position determination. The 65 wires in each plane were interconnected with resistors to obtain a suitable *RC* delay. The position was determined by the difference in risetimes of the pulses induced in the wires by a neutron event measured at each side of the plane. The overall position resolution at the detector corresponded to 9×9 mm^2 (FWHM) and, with the chosen slits, the width of the direct beam was 20 mm in diameter at half maximum at the detector. Correction for background was done only for the samples in quartz cuvettes by subtracting an empty-cell spectrum from the dry samples and a spectrum from the pure H_2O-D_2O mixtures for the suspended samples. Small variations in the efficiency over the detector area were corrected for by dividing the data by a spectrum from an incoherently scattering sample ("flat" spectrum). Here, a 1-mm H_2O sample was used. Both corrections were performed pixel by pixel.

III. EXPERIMENTAL RESULTS

A. Data

After background and normalization corrections, the spectra were radially averaged. Data taken at $\lambda=2.2$ nm cover the q range 0.05–0.2 nm^{-1} and data taken at $\lambda=0.6$ nm from $q=0.1$ to 0.9 nm^{-1}. The scale factor between these sets of data was determined approximately by the ratio of the integrated scattering from a 1-mm H_2O sample[14] with the two wavelength configurations. However, in the least-squares-fitting routine the scale factors were left as free parameters and were found to settle within $\pm10\%$ of the experimentally determined value.

Figure 1 shows a double-logarithmic representation of the radial averaged scattering curves for the four dry samples (F1–F5) with increasing densities and the H_2O-D_2O dispersed samples with roughly the same density. The scattering curves have the same overall shape. The slope increases at higher q and decreases at lower q, the latter being the only region where a significant density dependence was found. Qualitatively, the observed line shapes conform with the intuitive guess that the low-q data

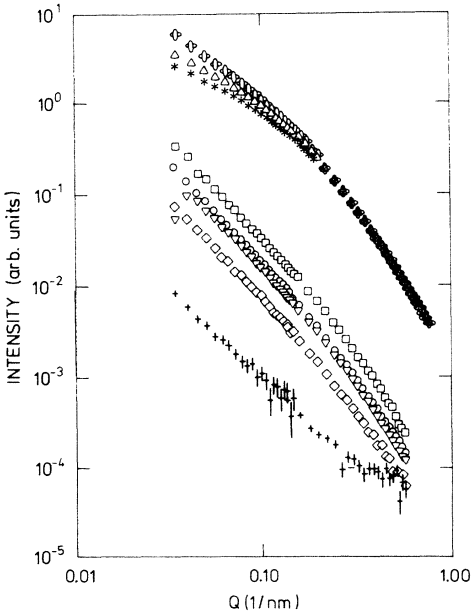

FIG. 1. Double-logarithmic representation of scattering curves for all samples measured. The data are shown in original form, only corrected for background and detector efficiency. The upper four curves are from the dry samples with varying densities: △, 0.13 g/cm^3; △, 0.17 g/cm^3; △, 0.34 g/cm; *, 0.45 g/cm^3. The lower five curves are from the water-dispersed samples with varying contrast ($[D_2O]/[H_2O]$ ratio): □, 8%; ○, 0%; △, 100%; ◇, 25%; +, 50% (by weight).

($q\xi \ll 1$, where ξ is a typical cluster size) should show a trend toward saturation due to finite aggregate size.

B. H_2O-D_2O contrast variation

A contrast-variation method using H_2O-D_2O infusion can be evaluated to determine whether the particles have open structures accessible to the dispersing water or closed pores remaining empty under the suspension. In the latter case, the system SiO_2 + empty pores + H_2O-D_2O would have no simple contrast-matching point upon continuously varying the $[H_2O]/[D_2O]$ relative concentration. On the other hand, if the liquid fills all the pores, one has simply two scattering-length densities, namely that in the SiO_2 (ρ_s) and that in the H_2O-D_2O mixture (ρ_0). Thus, a well-defined matching point ($\rho_0=\rho_s$) implies that there are no empty pores.

Figure 2 shows the square root of normalized intensity versus contrast for $q=0.3$ nm^{-1}. From this we conclude that no significant deviation from a linear relationship can be deduced, i.e., no empty pores remain unfilled by the dispersing water. The match point is determined to ≈ 66 wt. % D_2O in H_2O, corresponding to a scattering-length density[15] of 40.4×10^{-12} cm/nm^3 and a SiO_2 density in the primary particles of 2.55 g/cm^3, in agreement with table values.

C. Size distribution

A representation of the data in a Guinier plot [$\log(I)$ versus q^2], as shown for a typical sample in Fig. 3, clearly indicates that there is no simple characteristic length scale to be deduced from the data, except possibly the Guinier radius corresponding to the limiting slope at small q. Scattering curves of this kind are often analyzed as scattering from a hypothetical distribution of spherical particles with a distribution of radii.[16] This approach can be used to represent the present data for the dry samples, but the parameters derived in this fashion do not have any obvious microscopic significance, e.g., the obtained particle-size averages show a very strong dependence on

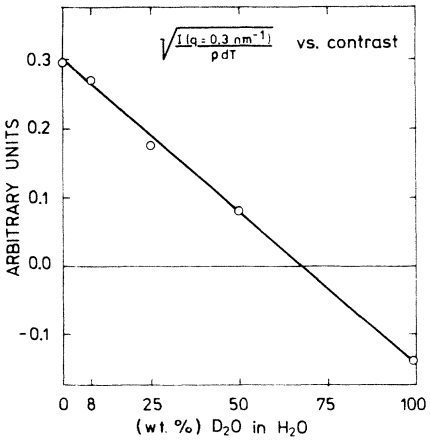

FIG. 2. Plot of square root of normalized scattered intensity at constant $q=0.3$ nm^{-1} versus contrast for the water-dispersed samples. The existence of a well-defined matching point shows that the clusters are fully dispersed, i.e., no empty pores remain unfilled.

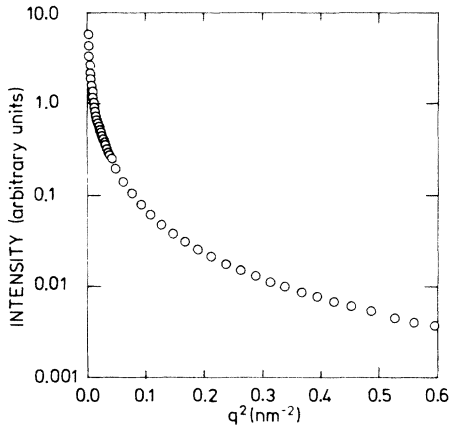

FIG. 3. Guinier plot ($\log I$ vs q^2) for a representative sample. As may be seen, no simple characteristic length scale can be deduced from the data.

density, and yield a narrow distribution of relatively small particles, whose peek occurs at (≈ 30 nm) for the highest densities and a broader distribution of larger particles for the uncompressed samples. This picture is not in agreement with electron micrographs taken from the samples.

We argue that a more natural interpretation of the scattering curves can be based on the assumption of power-law correlations between the centers of small fairly monodisperse spherical units ($R\simeq 2.0$ nm). As will be shown below, this gives a consistent description of the data at all densities.

IV. SCATTERING FUNCTION

As discussed qualitatively in the Introduction, the assumption of scale invariance implies the simple but important power-law form $I(q)\propto q^{-d_f}$ for the scattering function. In real systems of aggregates the scale invariance is limited both at large r (by the finite size of the cluster, or by the entanglement of the clusters) and at small r by the finite size of the particles making up the aggregate. The qualitative effects of these cutoffs are illustrated schematically in Fig. 4, and below we derive analytic expressions for $S(q)$ which include the effects. The scattering function $I(q)$ per particle is given by

$$I(q)=\frac{1}{N}\sum_{i,j}\int d\mathbf{r}\int d\mathbf{r}'\rho(\mathbf{r}-\mathbf{R}_i)\rho(\mathbf{r}'-\mathbf{R}_j)e^{i\mathbf{q}\cdot(\mathbf{r}-\mathbf{r}')}\,, \tag{4.1}$$

where N denotes the total number of particles, the sum is over all pairs of particles, and $\rho(\mathbf{r}-\mathbf{R}_i)$ denotes the scattering-length density of a constituent particle situated at $\mathbf{R}_i$ minus the average scattering-length density of the macroscopic sample. All the particles are assumed to be identical here, although the extension to polydisperse systems is trivial. We may rewrite Eq. (4.1) as

$$I(q)=v_0^2(\rho_s-\rho_0)^2f^2(\mathbf{q})S(\mathbf{q})\,, \tag{4.2}$$

where ρ_s is the scattering-length density averaged over a particle of volume v_0, ρ_0 is the scattering-length density of the embedding medium, and $f(\mathbf{q})$ is the single-particle

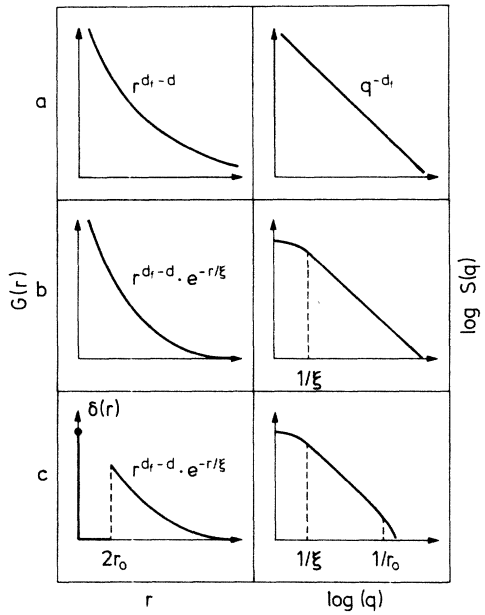

FIG. 4. Correlation function $G(r)$ and corresponding scattering function $S(q)$ for a fractal structure. (a) Infinite cluster, (b) cluster with upper cutoff at $r\simeq\xi$, and (c) cluster with both upper and lower cutoffs. The particle centers cannot approach closer than a radius $2r_0$ and the simplest corrections for this is to set $G(r)$ to zero for $0<r\leq 2r_0$.

form factor given by

$$f(\mathbf{q})=\frac{1}{v_0(\rho_s-\rho_0)}\int \rho(\mathbf{r})e^{i\mathbf{q}\cdot\mathbf{r}}d\mathbf{r}\ . \tag{4.3}$$

$f(\mathbf{q})$ is thus normalized so that it goes to unity at $\mathbf{q}=\mathbf{0}$. $S(\mathbf{q})$ is the structure factor of the particle centers, given by

$$S(\mathbf{q})=\frac{1}{N}\sum_{i,j}e^{-i\mathbf{q}\cdot(\mathbf{R}_i-\mathbf{R}_j)}\ , \tag{4.4}$$

which may be written in terms of the particle pair-correlation function $G(\mathbf{r})$ by

$$S(\mathbf{q})=N\int G(\mathbf{r})e^{-i\mathbf{q}\cdot\mathbf{r}}d\mathbf{r}\ , \tag{4.5a}$$

$$G(\mathbf{r})=\delta(\mathbf{r})+G_{\rm diff}(\mathbf{r})\ . \tag{4.5b}$$

For a fractal object of fractal dimension d_f it may be easily shown that the definition $N(R)\sim R^{d_f}$ [where $N(R)$ is the number of particles within a radius R around a given particle] leads to

$$G_{\rm diff}(\mathbf{r})=A/r^{d-d_f}\ , \tag{4.6}$$

where A is a constant. However, for the actual systems we are considering, where the aggregates have a finite cluster size and, furthermore, the clusters may be quite entangled, we have to weight $G_{\rm diff}(r)$ with the probability that the fractal correlations around a given particle exist for distances greater than or equal to r. We may represent this by a scaling function $F(r/\xi)$ characterized by a single effective cutoff length ξ, and for simplicity we assume an exponential form for this function. [More complicated forms of the scaling function involving exponentials of arbitrary powers of r/ξ could be considered, as has been done by Aharony *et al.*[17] for the case of spin correlations on percolating clusters. The advantage of the present form is that it lends itself to an analytic form for $S(q)$ which may be used to fit the data. Furthermore, the fact that it leads to internally consistent values of the fitted parameters, as we shall see, did not seem to necessitate exploration of more complicated forms of this scaling function.]

Thus, we write, instead of Eq. (4.6),

$$G_{\rm diff}(r)=(A/r^{d-d_f})\exp(-r/\xi)\ . \tag{4.7}$$

Substituting the expression in Eq. (4.5) and carrying out the Fourier transform yields

$$S(q)=1+\frac{C(d_f-1)\Gamma(d_f-1)\xi^{d_f}}{(1+q^2\xi^2)^{d_f/2}}\frac{(1+q^2\xi^2)^{1/2}}{q\xi}\times\frac{\sin[(d_f-1)\arctan(q\xi)]}{d_f-1}\ , \tag{4.8}$$

where C is a constant. Note that the second term behaves—for $q\xi\gg 1$—as q^{-d_f}, as expected from the fractal nature of the correlations between the particles. For very large q the first term will dominate, and when multiplied by $f^2(q)$ [see Eq. (4.2)] will lead to Porod-type scattering characteristic of scattering from the individual particles, which are assumed to have a well-defined surface area. However, for the q ranges measured in this experiment, this term is negligible compared to the second term in Eq. (4.8). For $q\xi\ll 1$, $S(q)$ has the expected saturation behavior and leads to a value proportional to ξ^{d_f} as $q\to 0$. For spherical, monodisperse particles, as is the case for the aggregates studied here, the form factor may be written as

$$f(q)=3\left[\frac{\sin(qr_0)-qr_0\cos(qr_0)}{(qr_0)^3}\right]\ , \tag{4.9a}$$

where r_0 is the particle radius.

For the particle sizes and q ranges relevant to the present experiment, one may equivalently use the Guinier approximation to this, which is

$$f^2(q)\simeq\exp(-\tfrac{1}{5}q^2r_0^2)\ . \tag{4.9b}$$

Equations (4.8) and (4.9b) were used together with Eq. (4.2), after folding with the instrumental resolution, to fit the experimental data in terms of the adjustable parameters d_f, r_0, ξ, and C, as will be discussed in the next section.

It should be noted that Eq. (4.7) does not properly describe the behavior of $G_{\rm diff}(r)$ at small r. For instance, the particle centers cannot approach closer than a radius $2r_0$. The simplest improvement one can make is simply to set $G_{\rm diff}(r)$ as given by Eq. (4.7) by zero for $r\leq 2r_0$. In this case $S(q)$ may still be written in analytical form, i.e.,

$$S(q)=1+\frac{C(d_f-1)\xi^{d_f}}{(1+q^2\xi^2)^{d_f/2}}\frac{(1+q^2\xi^2)^{1/2}}{q\xi}$$

$$\times\mathrm{Im}[[\Gamma(d_f-1,\ (2r_0/\xi_0)(1-iq\xi))]\{\cos[(d_f-1)\arctan(q\xi)]+i\sin[(d_f-1)\arctan(q\xi)]\}/(d_f-1)] \ . \quad (4.10)$$

Here, $\Gamma(\alpha,z)$ is the incomplete Γ function with complex argument[18] defined by the complex integral

$$\Gamma(\alpha,z)\equiv\int_z^\infty w^{\alpha-1}\exp(-w)dw \ . \quad (4.11)$$

The form (4.10) will differ significantly from that given by Eq. (4.8) only for $qr_0\geq 1$, and thus the present experimental data is not sensitive to the difference between the two forms.

V. ANALYSIS AND DISCUSSION

Equation (4.2), together with the different forms for $S(q)$, was used to make least-squares fits to the data. The instrumental resolution was taken into account in the fitting procedure via a convolution of $I(q)$ with the SANS-system resolution function, $R(q,q')$,

$$I_{\mathrm{obs}}(q)=\int dq' I(q')R(q,q') \ . \quad (5.1)$$

$R(q,q')$ describes the probability of detecting a scattering event with momentum transfer q at the momentum transfer q', and it was obtained by assuming a two-dimensional Gaussian resolution function in the detector plane that was radially averaged. $R(q,q')$ has the form

$$R(q,q')=\frac{q'}{\sigma^2(q)}\exp\left[-\frac{q^2+(q')^2}{2\sigma^2(q)}\right]I_0(q'q/\sigma^2(q)) \ , \quad (5.2)$$

where $I_0(x)$ is the modified Bessel function of the first kind and order 0. The q-dependent $\sigma^2(q)$ is approximated by a quadratic form

$$\sigma^2(q)=A+Bq^2 \ . \quad (5.3)$$

A was measured from the direct-beam profile to $A=6.2\times10^{-5}$ nm^{-2} and B was estimated from the wavelength resolution, $\Delta\lambda/\lambda=18\%$ (FWHM), yielding $B=7.2\times10^{-3}$.

The two models (4.8) and (4.10) were both used to make least-squares fits to the data. With the use of (4.10) one obtains fits with χ^2 around half of the value compared to (4.8), but the comparable parameters—d_f, r_0, and ξ—did not change markedly from one model to another. Figure 5 shows model (4.10) fitted to data from a representative set of samples and Table I gives the values for the obtained parameters.

From Table I we conclude that $d_f=2.61\pm0.1$, independent of the macroscopic density for the dry samples, while for the dispersed samples, $d_f=2.34\pm0.1$. The lower value in the latter case may be due to the decanting procedure in the sample preparation or the infused water may cause a slight opening of the structure.

The primary particle radius r_0 seems to settle around 2 nm for all samples, while the upper cutoff ξ is systematically related to the macroscopic density ρ. ξ is found to scale roughly with $\rho^{-1/3}$, as expected if the degree of entanglement of the clusters scales down linearly with the average distance between clusters.

The values for the constant C do not vary significantly, indicating that the nearest-neighbor correlations between primary particles are not changed. A determination of the coordination number for these units is, in principle, possible if the scattering curves were extended to higher q values to obtain better estimates for C and r_0.

The scale factor A_1, normalized to the number of scatterers and corrected for transmission and, for the dispersed samples, the contrast, also appears to be fairly constant for all samples. The fluctuations for the dispersed samples are most likely due to inaccuracies in the determination of the SiO_2 concentration in these samples. This implies that the intensity for $q=0$ scales as expected for a fractal system, $I(q=0)\propto\xi^{d_f}$ [see Eq. (4.8) or (4.10)], giving an independent test of the consistency of the model.

VI. CONCLUSION

We have measured the scattering function $S(q)$ for a series of samples of aggregated silica particles of varying densities. The densities range from extremely low values of 0.008 g/cm^3 (corresponding to the water-dispersed aggregates) to 0.45 g/cm^3 (corresponding to the most

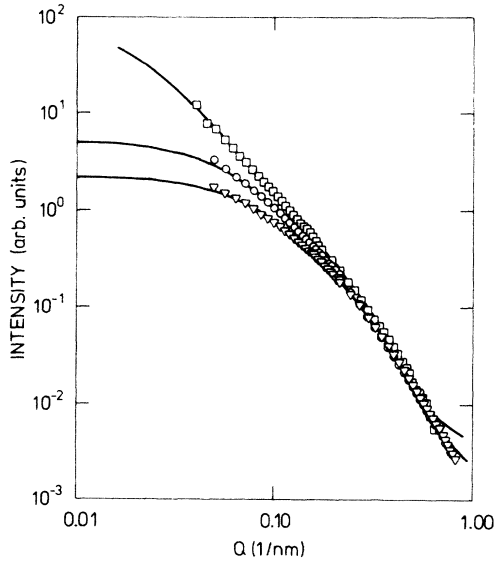

FIG. 5. Three representative scattering curves with the fitted model shown (solid curve). From above: □, water dispersed, 0.01 g/cm^3; ○, dry, 0.13 g/cm^3; △, dry, 0.45 g/cm^3. The water-dispersed data are scaled by the ratio of prefactors, A, obtained by the fitting routine. Note the logarithmic scales.

TABLE I. Fit results. Results from least-squares fits of Eq. (4.2) where Eqs. (4.9a) and (4.10) have been inserted. The prefactor $v_0^2(\rho_s-\rho_0)^2$ in (4.2) is represented by A_1, which here is shown corrected for sample density ρ, thickness d, transmission T, and, for the dispersed samples, contrast $\sigma=[(\rho_{SiO_2}-\rho_{D_2O/H_2O})/\rho_{SiO_2}]^2$ obtained from Fig. 2.

Sample F: dry D: dispersed	Density (g/cm^3)	$A_1/(\rho dT\sigma)$	C (10^{-3})	ξ (nm)	r_0 (nm)	d_f
F1	0.13	0.96±0.1	1.02±0.07	13.2±0.6	1.9±0.1	2.60±0.03
F2	0.17	0.92±0.1	0.96±0.07	12.1±0.4	1.9±0.1	2.65±0.03
F3	0.34	0.90±0.1	1.02±0.06	10.4±0.3	1.9±0.1	2.64±0.03
F5	0.45	0.94±0.1	1.32±0.11	10.0±0.4	1.8±0.1	2.55±0.04
D11	0.008	1.27±0.2	0.91±0.06	31 ±2	2.3±0.1	2.41±0.02
D31	0.006	1.79±0.2	1.02±0.14	56 ±10	2.4±0.1	2.27±0.04
D41	0.010	1.48±0.2	1.43±0.14	52 ±9	2.2±0.1	2.29±0.03
D51	0.008	0.92±0.2	0.91±0.07	42 ±4	2.3±0.1	2.38±0.02

compressed disk). It is the ability to study the fractal nature of this system over such a wide range of densities that is one of the unique features of our experiment. In terms of the experiment we have established the usefulness of the concept of an upper length-scale cutoff ξ, which must be used to analyze scattering data from real (as opposed to mathematical) fractals, as in the case where the aggregated clusters have a finite size or become entangled, thus losing the power-law correlations which exist on a single cluster. The essence of this picture may thus be applied to systems such as polymer gels or other structures where the power-law correlations decay at large length scales.

The consistency of our use of the parameter ξ is seen both from the behavior of ξ as a function of the macroscopic density and of scaling behavior of the intensity in terms of ξ. In the former case we find that ξ scales roughly as $\rho^{-1/3}$, which gives credence to the concept of the degree of entanglement of the clusters scaling down linearly with the average distance between clusters. In the latter case the fact that $I(q=0)\propto\xi^{d_f}$, where both parameters, ξ and d_f, have been determined from our fits, constitutes an independent test of the internal consistency of our analysis in terms of the fractal nature of the aggregates.

We now turn to a discussion of the value obtained for d_f. It is interesting that d_f appears to be independent of the macroscopic density, except for a slight decrease in the case of the low-density water-suspended samples. This value is close to the value obtained in computer simulations of the diffusion-limited–aggregation process in three dimensions. In the case of slow aggregation of colloidal gold particles, Weiz *et al.*[10] measured a value of $d_f=2.05$. This is close to the value 2.12 obtained by Schaefer *et al.* for aggregates of collodial silica particles. Fast aggregation of colloidal gold particles, on the other hand, yields a value of $d_f=1.8$. This latter value is in good agreement with computer simulations based on the cluster-cluster model. In the study of protein aggregates, Feder *et al.* deduce a value for $d_f=2.56$. The growth models used by Ulrich and Riehl[11] to analyze their light scattering data from Cab-O-Sil in the early stage of the aggregate formation are consistent with a fairly high fractal dimension (≈ 2.5). They observe a crossover to less dense growth at an aggregate size of $\approx 50\,000$ particles, which corresponds to a length scale much larger than is accessible in the present experiment. It is not yet clear whether these various values for d_f are universal and characteristic of different mechanisms for aggregation. If so, d_f provides a signature for the aggregation process and may thus be useful in studying and characterizing such systems.

Further studies of the fractal nature of aggregates are needed to establish this point. In addition, we point out that this present system may provide a convenient experimental testing ground for further current theoretical ideas concerning the physical properties of fractals. In particular, it would be of interest to measure also the spectral dimension related to the low-frequency dynamics of such systems.

ACKNOWLEDGMENTS

The authors have benefited from helpful discussions with Tom Witten, Phil Pincus, and David Weitz. One of us (S.K.S.) thanks the John Simon Guggenheim Memorial Foundation for financial aid during the tenure of which this work was carried out, and also thanks Risø National Laboratory for their hospitality during his visit. The help from F. W. Poulsen in the sample preparation is gratefully acknowledged.

[1]M. von Smoluchowski, Phys. Z. **17**, 557 (1916); **17**, 585 (1916).
[2]S. R. Forrest and T. A. Witten, J. Phys. A **12**, L109 (1979).
[3]T. A. Witten and L. M. Sander, Phys. Rev. Lett. **47**, 1400 (1981).
[4]T. A. Witten and L. M. Sander, Phys. Rev. B **27**, 5686 (1983).
[5]B. B. Mandelbrot, *The Fractal Geometry of Nature* (Freeman, San Francisco, 1983).
[6]Cab-O-Sil (grade M5) is a trademark of the Cabot Corporation; the Alfasil sample was stock no. D89376 (Alfa Products 1981 Catalog).
[7]S. K. Sinha, T. Freltoft, and J. K. Kjems, in *Kinetics of Aggregation and Gelation*, edited by F. Family and D. Landau

(North-Holland, Amsterdam, 1984), pp. 87–90.
[8]D. W. Schaefer, J. E. Martin, P. Wiltzius, and D. S. Cannell, Phys. Rev. Lett. **52**, 2371 (1984).
[9]D. A. Weitz, and M. Oliveria, Phys. Rev. Lett. **52**, 1433 (1983).
[10]D. A. Weitz, J. S. Huang, M. Y. Lin, and J. Sung, Phys. Rev. Lett. **53**, 1657 (1984).
[11]G. D. Ulrich and J. W. Riehl, J. Colloid. Interface Sci. **87**, 257 (1982).
[12]J. K. Kjems, R. Bauer, B. Breiting, P. Christensen, T. Freltoft, L. G. Jensen, and J. Linderholm, in *Proceedings of the International Conference on Neutron Scattering in the 'Nineties* (IAEA, Vienna, 1985), pp. 495–501.
[13]J. K. Kjems, R. Bauer, B. Breiting, and A. Thuesen, in *Proceedings of the International Conference on Neutron Scattering in the 'Nineties,* Ref. 12, pp. 489–495.
[14]R. P. May, K. Ibel, and J. Haas, J. Appl. Crystallogr. **15**, 15 (1982).
[15]L. Koester, H. Rauch, M. Herkens, and K. Schröder, in Summary of Neutron Scattering Lengths, Kernforschungsanlage Jülich Bericht Jül-1755, 1981 (unpublished).
[16]P. W. Schmidt, J. Appl. Crystallogr. **15**, 567 (1982).
[17]A. Aharony, Y. Gefen, and Y. Kantor, J. Stat. Phys. **36**, 767 (1984).
[18]F. W. Schäfke, *Einführung in die Theorie der Speziellen Funktionen der mathematischen Physik* (Springer, Berlin, 1963).